# Periodicity-Induced Symmetry Breaking in a Fano Lattice: Hybridization and Tight-Binding Regimes

Chen Yan and Olivier J. F. Martin*

Nanophotonics and Metrology Laboratory, Swiss Federal Institute of Technology (EPFL), CH-1015 Lausanne, Switzerland

ABSTRACT We investigate experimentally and theoretically the role of periodicity on the optical response of dolmen plasmonic arrays that exhibit a Fano line shape. Contrary to previous works on single nanostructures, this study deals with the in-plane near-field coupling between adjacent unit cells. By making an analogy to the electronic properties of atoms in the tight-binding model, specific behaviors of photonic states are investigated numerically as a function of the structural asymmetry for different coupling directions. These predictions are verified experimentally with dark-field measurements on nanostructure arrays which exhibit high tunability and fine control of their spectral features as a function of the lattice constants. These effects, originated from symmetry-breaking and selective excitation of the subradiant mode, provide additional degree of freedom for tuning the spectral response and can be used for the sensitive detection of local perturbations. This study provides a general understanding of the near-field interactions in Fano resonant lattices that can be used for the design of plasmonic nanostructures and planar metamaterials.
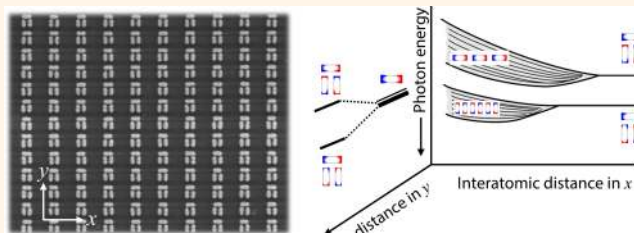
KEYWORDS: plasmonics · Fano resonance · periodicity · symmetry-breaking · hybridization · tight-binding regime · radiance sensing

O ver the past decade, localized surface plasmon resonances have attracted significant attention thanks to their ability to confine and enhance electromagnetic fields at the nanoscale.[1] These properties are enabled by the collective electrons oscillations in metallic nanostructures. Depending on how strong the radiation associated with these oscillations can be coupled into free space, a plasmon resonance can be either superradiant or subradiant.[2] Specific geometries, such as two parallel nanorods,[3,4] metallic rings,[5] or well-arranged nanoparticle clusters,[6] can support high-order plasmonic modes with a subradiant character. By combining those subradiant modes with a radiative plasmonic resonance (superradiant mode), the system becomes extremely sensitive to local perturbations and exhibits a unique asymmetric line shape, known as Fano line shape.[7−10] Recently, it has been shown that optical Fano resonant systems can dramatically enhance the performances of nanophotonic applications such as nanorulers,[11,12] surface-enhanced Raman spectroscopy,[13,14] and molecular detection.[15,16]

Optical Fano resonances have been investigated in various *individual* plasmonic nanostructures[4,5,17,18] and metamaterials based on plasmonic constituents, including nanoparticles aggregates,[6] diffraction gratings,[19] and hole or particle arrays.[14,20,21] However, large periodic *arrays* are commonly used for experimental investigations. When the periodicity is larger than the working wavelength range, Wood's anomalies[22,23] arise from surface lattice resonances[21,24] and result in extremely narrow reflection dips or extraordinary transmission lines.[25−29] Since the Wood's anomaly strongly depends on the array period, it can interfere with other spectral features of interest related to the coupling between neighboring elements which also depend on the periodicity; it is then better to avoid working near the Wood's anomaly by fabricating dense arrays with periodicity smaller than the working wavelength. Such a nondiffractive array provides better signal-to-noise ratio than a single structure, while the optical response can still be considered the same as that of a single structure.[30−32] However, when the spacing between adjacent unit structures is
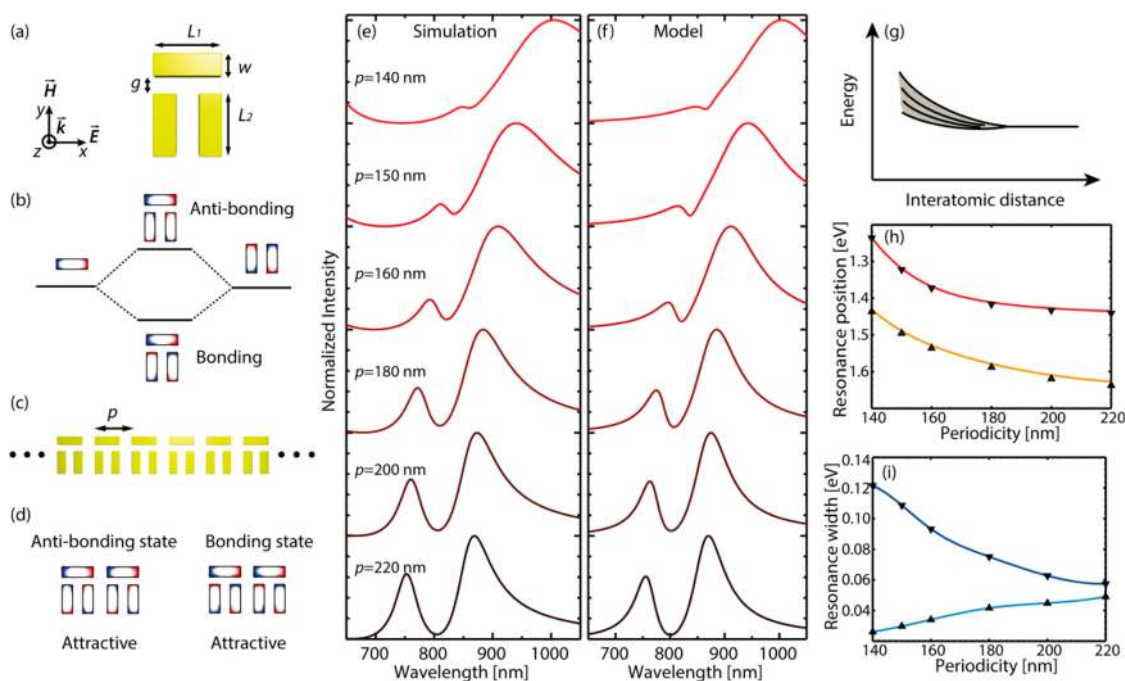
Figure 1. (a) Sketch of a dolmen plasmonic unit cell with incident light polarized in the x-direction, L_1 = 120 nm, L_2 = 110 nm, g = 25 nm, w = 40 nm. (b) Energy-state diagram with the splitting and strong hybridization between dipolar radiative resonances and quadrupolar nonradiative resonances. Blue and red show the charge distribution at the resonance condition. (c) Schematics of the side-coupled 1D dolmen lattice. (d) Charge distribution and Coulomb force between neighboring nanostructures under the bonding state and the antibonding state. (e, f) Calculated reflectance spectra and fitting curves for varying periodicities from p = 220 to 140 nm. (g) Optical analogy for the formation of energy bands in solid-state physics when the interatomic distance changes. (h) Extracted resonance position of superradiant and subradiant modes as a function of periodicity. (i) Extracted resonance width for superradiant and subradiant modes as a function of periodicity.

small enough, near-field interactions cannot be neglected anymore[19,30,32,33] and can play an important role in the observed spectral features. For example, near-field interactions are the driving mechanism for plasmonic sensing,[31] surface enhanced Raman scattering,[34] and surface enhanced infrared absorption.[14]

A second critical factor for engineering the spectral response is the symmetry of the design. It is well-known that the symmetry of a system not only defines the modes it can support but also determines whether these modes have a subradiant (nonradiative or long decay time) or superradiant (radiative or short decay time) character.[35] For example, in radio frequency metamaterials, symmetry-breaking can result in the excitation of trapped modes with a high quality factor,[36] symmetry-breaking in ring–disk or core–shell nanostructures can also enable the coupling between dipolar and multipolar modes.[37,38] The latter higher order plasmon resonances are characterized by a subradiant nature resulting in a tunable Fano resonance. Other systems, including nanowire lattices,[19] metallic shells,[20] and aperture arrays[31] also exhibit subradiant features, although the link between their periodicity and the asymmetry in their spectral response has not yet been established.

In this work, we address this issue of near-field interactions in a dense plasmonic array by exploring

in the visible optical range a dolmen array with varying periodicities; we show that the response of this system follows different regimes: the hybridization regime and the tight-binding regime. The dolmen structure is used as building block for the entire study, since it supports a Fano resonance as individual nanostructure as well as exhibiting a strong polarization and geometry dependence.[3,17,39] The dolmen unit cell under study consists of three gold nanorods arranged as shown in Figure 1a. The single nanorod along the x-direction supports a dipolar resonance (superradiant mode), whereas the parallel nanorod pair along the y-direction supports a quadrupolar resonance (subradiant mode) where the charges oscillate out of phase, Figure 1b. The subradiant mode does not interact with free space and can only be excited by the near-field of the single nanorod. The coherent coupling between the superradiant and subradiant resonances in this system produces an optical Fano resonance,[8,17] whose line shape can be tuned by changing the gap size.[3,17] In our case, the gap is set to be smaller than 30 nm to ensure a large field overlap and, therefore, a strong coupling between both modes. In terms of energy-state diagram, the strong interaction results in a splitting of the original modes into two hybridized optical states.[40] Two resonance peaks occur in the low energy and high energy branches, as visible in the scattering

cross-section plot (Figure S1(b), Supporting Information), which we call bonding state and antibonding state, respectively Figure 1b.

In terms of structural symmetry, the unit cell is asymmetric along the *y*-direction due to the presence of the nanorods pair. Thus, we shall consider the interactions along the *x*- and the *y*-directions separately and for different periodicities. In the following, we show that an array in the *x*-direction acts as a chain of artificial atoms, *i.e.*, the optical modes associated with each structure in the array couple together to produce an optical potential similar to that of an atomic lattice. By reducing the periodicity, the system transforms from a quasi-single atomic regime to a tight-binding regime, where the localized resonances merge into a state extending over the entire crystal. In the *y*-direction, we first study a two dolmen system, both in the far-field and the near-field. The corresponding spectral features are first determined *ab initio* from the symmetry-breaking in the *y*-direction and further confirmed by analyzing the near-field behavior. After generalizing to an array, we experimentally demonstrate that the Fano resonance can be very effectively tuned using these effects. We finally discuss the possibility of implementing in that geometry the radiance sensing that was proposed in a previous work.[12] In particular, we show that it is possible to operate in the weak coupling regime in order to reach high sensitivity while preserving small gaps to produce a strong near-field confinement. This regime, controlled by the near-field interaction and the symmetry-breaking in a compact array, provides additional degree of freedom to control the spectral response and the Fano behavior of a collective system.

RESULTS AND DISCUSSION

The exact dolmen unit cell under study is illustrated in Figure 1a. The single nanorod along the *x*-direction has the dimensions $120 \times 40 \times 40$ nm^3, and the parallel nanorod pair along the *y*-direction has the dimensions $110 \times 40 \times 40$ nm^3. The separation between the two parallel nanorods is 40 nm, so that the left and right edges of a nanorod pair are perfectly aligned with the single nanorod. We use a periodic surface integral equation (SIE) method to calculate the optical properties for infinite arrays.[41,42] The dielectric function of gold is taken from Johnson and Christy.[43] The glass substrate has been taken into account in the simulation with a refractive index 1.5 and the incident condition is taken to be a planewave propagating in the *z*-direction with *x*-polarization.

Optical Properties of a Side Coupled Dolmen Array. A compact array of dolmen along the *x*-direction is first studied, as illustrated in Figure 1c. Because the dolmen structure is symmetric with respect to the *y*-axis, the side coupling does not significantly affect the coupling strength between the single nanorod and

the nanorod pair. However, as the periodicity decreases, there is a strong field overlap between the dipolar modes from neighboring structures as well as a strong field overlap between the quadrupolar modes caused by the topological arrangement. The nanorod along *x* on the top of the dolmen structures, oscillating in phase, exhibits a strong superradiant characteristic, while the assembly of parallel nanorod pairs, oscillating out-of-phase, induce a very small total dipole moment that causes the original subradiant mode to become even darker and narrower. These intramode interactions exhibit a collective dipolar and a collective quadrupolar character, which can be understood with an analogy to two atomic chains with additional coupling between them, as will be discussed in the next paragraph. In Figure 1e, we calculate the reflectance spectra for different 1D dolmen lattices aligned in the *x*-direction with periodicities varying from $p = 140$ to 220 nm. The spectral analysis reveals that the periodicity influences both the width and the central frequency of the collective dipolar and collective quadrupolar resonances. Similar to a solid-state atomic array, where a periodic potential allows the formation of electronic energy bands when the interatomic distance becomes comparable to the atomic size (Figure 1g),[44] here, the periodic metallic structures play the role of an optical potential and we observe the broadening of the resonance peak as the periodicity decreases, Figure 1e. Second, as the optical fields of neighboring structures start to overlap, the localized surface plasmon resonances in each particle begins to feel the oscillations of the free electrons from the adjacent structures. This effect occurs for very short separations, *e.g.*, in Figure 1h,i a periodicity of 180 nm corresponds to a spacing of 60 nm between neighboring elements. The intramode interaction is also visible in the charge distribution, which we compute from the normal component of the electric field 1 nm above the structure.[45] According to Figure 1d, the electrons in both dipolar and quadrupolar resonances feel an attractive Coulomb force from the neighboring structure. As a consequence, both collective states shift toward lower energies.

To quantitatively verify these behaviors, we use Gallinet's asymmetric modulation function to extract the exact parameters of the Fano-like line shape:[9,17]

$$R(\omega) = R_s(\omega) \cdot R_a(\omega)$$

$$= \frac{a^2}{\left(\dfrac{\omega^2 - \omega_s^2}{2\gamma_s \omega_s}\right)^2 + 1} \cdot \frac{\left(\dfrac{\omega^2 - \omega_a^2}{2\gamma_a \omega_a} + q\right)^2 + b}{\left(\dfrac{\omega^2 - \omega_a^2}{2\gamma_a \omega_a}\right)^2 + 1} \quad (1)$$

In this model, the symmetric Lorenztian envelope $R_s(\omega)$ represents the radiative contribution of superradiant modes while the asymmetric function $R_a(\omega)$ describes

TABLE 1. Extracted Parameters from the Asymmetric Modulation Model for Varying Periodicities

periodicity (nm)	ω_s (eV)	γ_s (eV)	ω_a (eV)	γ_a (eV)	b	q
220	1.435	0.057	1.627	0.049	0.249	1.537
200	1.427	0.063	1.609	0.045	0.296	1.334
180	1.411	0.075	1.579	0.042	0.244	0.945
160	1.368	0.093	1.529	0.034	0.280	0.466
150	1.319	0.109	1.489	0.030	0.357	0.180
140	1.235	0.122	1.431	0.026	0.550	0.0

the destructive or constructive interference due to the coherent coupling between superradiant the subradiant modes. The frequencies ω_s and ω_a give the resonance position, while the damping coefficients γ_s and γ_a give the width of the super- and subradiant resonances. The fitting curves are shown in Figure 1f, and the fitting parameters are given in Table 1. Parts h and i of Figure 1 provide a synthetic view of the results in Table 1. In a system composed of two atomic chains with additional coupling in between, there are mainly four coupling channels: dipole—dipole, quadrupole—quadrupole, dipole—quadrupole, and quadrupole—dipole. Figure 1h clearly shows the red-shift of both superradiant and subradiant resonances when reducing the periodicity, while the splitting between these two resonances remains relatively constant. The splitting energy gives quantitatively the strength of dipole—quadrupole interaction as approximately 0.2 eV, which is obviously constant since the coupling strength is determined by the fixed inner gap of the dolmen structure. The slope of the resonance position curves becomes significant for spacings smaller than 60 nm, and the shift exceeds the splitting energy of 0.2 eV when the spacing equals 20 nm ($p = 140$ nm). In that spacing domain, the dipole—dipole and quadrupole—quadrupole interactions dominate and the system can be understood in terms of the tight-binding atomic chain. This tight-binding behavior is further supported by Figure 1i where the width of the collective superradiant modes (in dark blue) increases dramatically when the spacing becomes smaller than 40 nm ($p = 140$ and 160 nm) and the damping coefficient γ_s of collective dipolar modes doubles when the spacing is 20 nm ($p = 140$ nm). On the other hand, for the subradiant mode (in light blue), the damping coefficient γ_a slightly decreases. Such counterintuitive tendency originates from the quadrupolar character of the mode supported by the parallel nanorod pair. Indeed, the radiative loss of this quadrupolar mode can only occur in the plane of the structure and this loss channel becomes less efficient when neighboring structures approach, leading to formation of a spatially extended state. This effect is in agreement with the fact that the darker is the subradiant mode, the narrower is the Fano dip.[10,17]

Coupling between Two Dolmens. In order to engineer a proper array for controlling the Fano resonance

strength, both the coupling direction and the dolmens orientation are important. Let us now analyze systems made of two coupled dolmens for five different configurations. The far-field spectra for different spacings are shown in Figures S2 and S3, Supporting Information. Again, two dolmens side coupled with the same orientation have the same behavior as discussed previously, Figure S2(a) (Supporting Information). However, for the inverted orientation in Figure S2(b) (Supporting Information), the spectrum does not vary much with the spacing. Such a system is very stable since the dipolar resonance supported by the single nanorod can hardly couple from the side to the neighboring quadrupolar resonance. The situation is different for the other three cases of coupling in the y-direction. When two dolmens are oriented foot-to-foot, Figure S3(a) (Supporting Information), it appears that the influence of spacing on the spectrum is negligible, indicating that the coupling between both quadrupolar modes is weak. When two dolmens are oriented head-to-head, Figure S3(b) (Supporting Information), the whole spectrum slightly blue-shifts since both dipolar modes repel each other. Although the Fano dip follows the blue-shift as well, its depth and width remain the same.

Now let us consider two dolmens coupled in the y-direction with the same orientation (Figure 2). By changing the spacing from 100 to 30 nm, the overall envelope does not shift, but the modulation damping depth of the Fano dip alters, as shown in Figure 2b. This is clear evidence of the tunability of the Fano resonance when varying the geometry. We have fabricated such structures by a lift-off process with e-beam lithography followed by 1 nm Cr adhesion layer and 40 nm Au thermal evaporation on a glass substrate. The inset in Figure 2d shows the scanning electron microscope image for two neighbor dolmens. The results of dark-field scattering measurements for three different spacings are shown in Figure 2d. The experimental spectra are somewhat broader and more damped than the simulated ones, which is most likely due to the structural roughness generated during the fabrication. Yet, the evolution of the Fano line shape when varying the spacing agrees very well with SIE simulations.

In Figure 2a, the charge distribution from a single dolmen indicates that when two dolmens are brought closer in the y-direction, the modes experience an attractive Coulomb force for the antibonding state; while the Coulomb force is repulsive for the bonding state. In total, this results in a reduction of the splitting strength and both resonance peaks slightly shift into the center when the spacing becomes smaller. To provide better insights into the system, we compute the 3D field distribution at three different wavelengths for the 60 nm spacing. Red to yellow represent the electric field intensity; and blue to purple represent the magnetic field intensity. At the wavelength of both
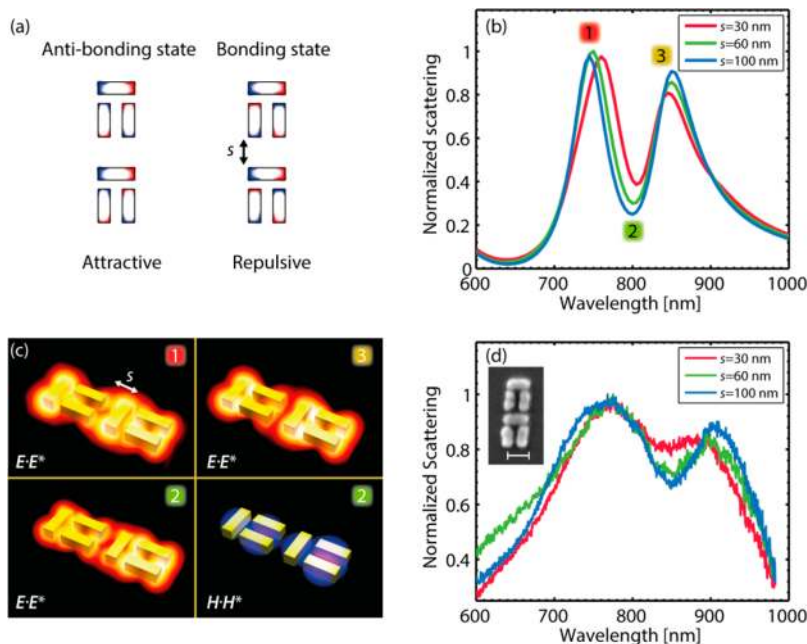
Figure 2. (a) Schematics of Coulomb interaction for two close dolmens aligned in the *y*-direction. (b) SIE simulation of the scattering spectra for an individual dolmen (black dashed line) and two coupled dolmens with different spacings *s* = 30, 60, and 100 nm. (c) Field distribution for two dolmens in near-field interaction for the spacing *s* = 60 nm. The electric field is shown in red to yellow, and the magnetic field is in blue to purple. (d) SEM image and dark-field measured scattering spectra for two dolmens with different spacings *s* = 30, 60, and 100 nm.

resonance peaks, the field is more confined around the single nanorod; while at the wavelength of the Fano dip, the field is strongly enhanced around the parallel nanorod pair due to the excitation of a quadrupolar mode (Figure 2c).[39] By changing the incident light frequency, we can selectively excite different hotspots in the structure. In addition, it is worth noticing that, at the wavelength of the dip, the strength of the quadrupolar mode of the first dolmen (on the left) is much weaker than that of the second one (on the right). This is evidenced in the magnetic field maps, where the magnetic hotspot is localized in the center of the nanorod pair. In this geometry, the additional near-field coupling between the quadrupolar mode of the first dolmen and the dipolar mode of the second dolmen must be considered. When the distance between two dolmens becomes identical to the inner gap size of the first dolmen, $s = g = 30$ nm, the dipolar oscillations prevents the excitation of the quadrupolar mode in the first dolmen, since the two nanorods are always driven in phase by the external field. However, the quadrupolar mode of the second dolmen does not experience any influence from its neighbor. Energy can be coupled into this subradiant mode and then coupled out indirectly through the superradiant mode, which results in an interference between the direct scattering from the single nanorod and the indirect optical path; the Fano dip is still present, even when the distance between two dolmens is as small as 30 nm.

Optical Properties of Dolmen Array Coupled in the *y*-Direction. Given the asymmetric behavior along the *y*-direction,

we generalize the two dolmens system for an array with full tunability of the Fano resonance. Now, the array is arranged as a chain with the mixture of two motifs elements. A schematic for a 1D dolmen array coupled in the *y*-direction is shown in Figure 3. In the same manner, we examine the near-field for three different arrays with spacings: $s = 30$, 60, and 100 nm. The computed magnetic fields for the superradiant and subradiant resonances, respectively, are shown in parts a and b of Figure 3. At the wavelength of the superradiant mode, most of the field is confined in the single nanorod, corresponding to the dipolar resonance. The field enhancement is approximately the same for all the cases. On the other hand, at the wavelength of the subradiant mode, although the quadrupolar modes are always excited on the nanorod pairs, the field enhancement varies significantly. When the spacing is equal to the inner gap size, $s = 30$ nm, the subradiant mode is completely forbidden. The field enhancement becomes substantial when the spacing is increased to 60 nm and the maximum field enhancement occurs when the spacing is large enough to ignore collective effects. Depending on how strong the symmetric-breaking is in such a 1D array, the system exhibits either Rabi splitting and strong hybridization or a narrow Fano line shape for a small asymmetric perturbation. Since all the quadrupolar modes are equivalent in the array, the optical Rabi splitting can vanish when the geometry is perfectly symmetric, as illustrated in the energy state diagram in Figure 3c. This behavior will be investigated for the system under study in the next paragraph.
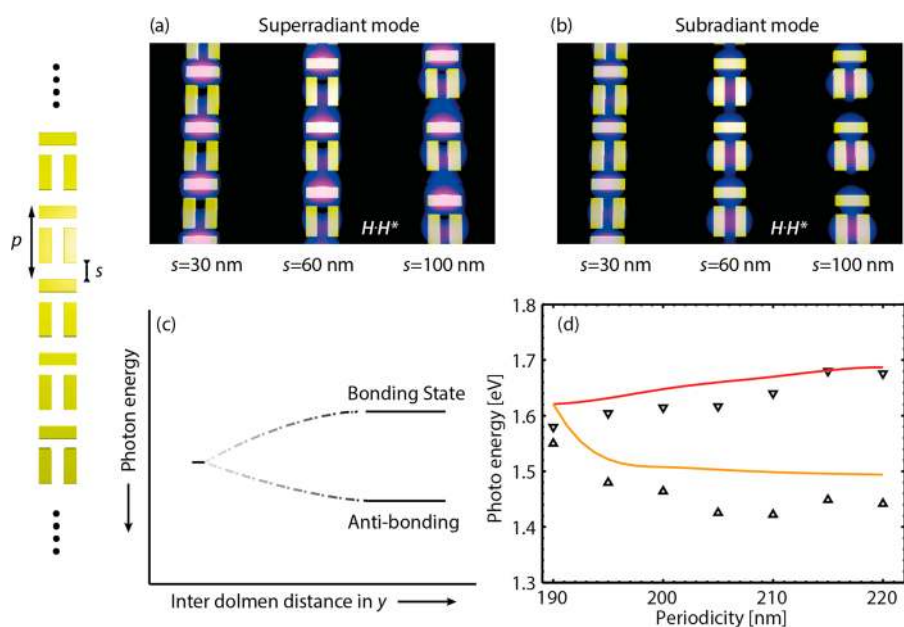
Figure 3. Schematics of a 1D dolmen lattice coupled in the *y*-direction. (a, b) Calculated magnetic field intensity distributions for different spacings: *s* = 30, 60, and 100 nm for the superradiant and subradiant resonances. (c) Energy-state diagram for the optical states when the lattice constant decreases. (d) Resonance peak position from SIE simulations (solid lines) and dark-field measurements (triangular dots) as a function of periodicity.
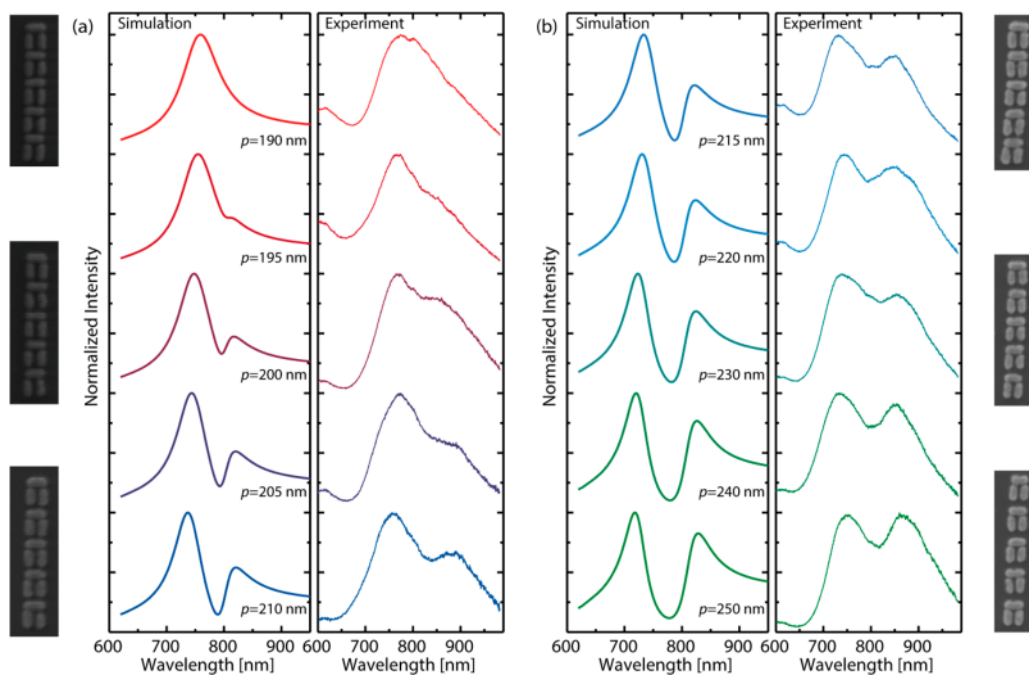

Figure 4. (a) SIE simulations and dark-field measurements of reflectance spectra for different dolmen lines aligned in the *y*-direction in the weak and intermediate coupling regimes, for a periodicity varying from *p* = 190 to 215 nm. (b) SIE simulations and dark-field reflectance measurements spectra in the strong coupling regime, for periodicity from *p* = 210 to 250 nm. The insets show the SEM images of the corresponding 1D dolmen array.

The ability to adjust the strength of subradiant resonances in the near-field hints that the Fano line shape visible in the far-field can also be controlled. This is evidenced in Figure 4, which presents normalized reflectance measurements as well as SIE simulations and SEM pictures for 10 different periodicities of dolmen arrays. The measured spectra agree very well with the calculated ones. The starting period *p* = 190 nm is chosen such that the distance between nearby dolmens is equal to the inner gap size, which corresponds to a perfectly symmetric configuration. The parallel nanorod pair feels exactly the same near-field interaction from the top and the bottom nanorods. These two nanorods, oriented along the *x*-direction, from neighboring unit

cells oscillate in phase and prevent the formation of quadrupolar subradiant modes, leading to a single Lorentizian resonance peak in Figure 4a. As soon as the symmetry is broken by increasing the period by 5 nm, we see a shoulder appearing on the red side of the main superradiant peak, which indicates the onset of interaction with the subradiant mode, even though the interaction strength is still very weak for such a small perturbation. The system transforms rapidly from the weak coupling to the strong coupling regime when the period is further increased from $p = 195$ to 215 nm. In the strong coupling regime, as shown in Figure 4b, the superradiant and subradiant modes strongly hybridize, and the splitting between bonding and antibonding states is maximum. The peak position in eV extracted for these states as a function of the periods is shown in Figure 3d. The solid lines correspond to the SIE simulation and the triangular dots correspond to the measurement. A 20 nm red shift is observed between calculations and measurements; it could be caused by overexposure or defects in the fabricated sample. However, the general trends match well; especially, both calculations and measurements exhibit a steady reduction of the splitting strength when the structures become symmetric. Furthermore, we observe that the relative intensity of the peak at the longer wavelength increases with respect to the peak at shorter wavelength in the strong coupling regime, which is a similar effect of asymmetry reversal as that observed in metallic double gratings.[17]

In the weak coupling and intermediate coupling regimes, Figure 4a, the resulting spectral profiles are modulated by an asymmetric line shape characteristic of Fano resonances, where the coupling strength can be characterized by the effective damping depth b_{eff}. The b_{eff} factor, extracted by fitting the spectrum with the Gallinet asymmetric modulation model, eq 1,[9,17] is defined as the minimum value of the asymmetric function. The expression is written as

$$b_{eff} = \frac{1}{2}(1+b+q)^2 + \frac{1}{2}\sqrt{1 - 2b + b^2 + 2q^2 + 2bq^2 + q^4}$$
(2)

where b and q are the modulation damping and asymmetric parameters given in the original model.[9] The value of the damping depth depends on the coupling strength and the intrinsic loss of the system: $b_{eff} = 1$ corresponds to no coupling between the superradiant mode and the subradiant mode, while $b_{eff} = 0$ corresponds to strong coupling in an energy-conservative system. In Figure 5, we plot the effective damping depth from experimental results (circular dots) as a function of periodicity. Compared with simulation results (blue solid line), all values are shifted up, but the response versus periodicity remains the same. A larger slope is obtained for small periodicities, as highlighted in the orange band, since the geometry
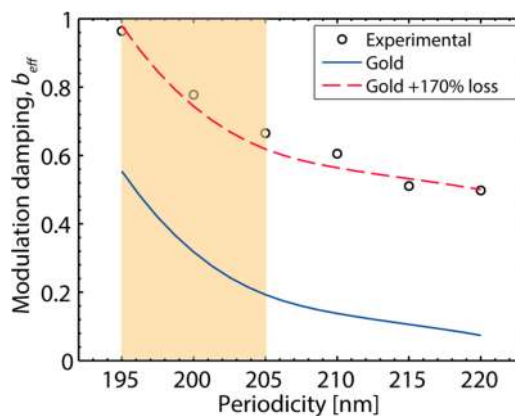

Figure 5. Effective modulation damping depth b_{eff} extracted from the asymmetric mode, eq 2, as a function of the periodicity. Measured results (circular dots), SIE simulations (blue solid line), and simulations using 2.7 times losses for gold (red dashed line) are shown.

is close to the symmetry-breaking condition. For those periodicities between 195 and 205 nm, the Fano resonance is in a weak coupling regime where the energy of the subradiant mode increases monotonically.[12] The value of effective modulation damping retrieved from the far-field spectra provides insights into the local field enhancement of the subradiant mode, which is crucial for the design of Fano resonant structures for nanophotonic applications. For instance, a strong variation of intensity at the Fano dip implies the excitation of subradiant modes leading to an extreme sensitivity to local perturbations that can be either geometrical or environmental.[11,12,31]

Finally, we modify the intrinsic loss of gold in the SIE simulation to verify the existence of sensitivity in a nonideal system. By increasing the imaginary part of the gold permittivity by 1.7 times, we are able to match the curve with the measured results, as shown as a red dashed line in Figure 5. The strong slope for small periods is conserved, since the sensitivity is essentially determined by the subradiant feature of the system. Although this value of modified intrinsic loss may appear quite large,[31] it accounts for three different phenomena. First, the properties of gold at the nanoscale are different from the bulk, since the polycrystalline nanostructures can cause strong electron scattering from the grain boundaries.[46] Second, the surface roughness and defect generated from the lithographic fabrication process lead to additional loss channels. Last, as a consequence of the structural inhomogeneous, the measured spectra suffer from inhomogeneous broadening, leading to damped Fano dips and broadened features.

CONCLUSIONS

In summary, periodic arrays of dolmen-like plasmonic nanostructures supporting Fano resonances in the optical spectral range have been investigated both

numerically and experimentally. We have shown that different near-field coupling mechanisms can occur in different directions and for specific orientations, giving rise to the overall response of the system. Depending on the interaction between neighboring elements, the far-field response of these plasmonic systems can evolved into a regime that is akin to a tight-binding regime or to a hybridization regime. Moreover, since the nature of the Fano line shape is linked with the excitation of subradiant modes in the near-field, these mechanisms of tuning the far-field response can be generalized to an array. High tunability and full control over the different spectral features have been demonstrated by merely varying the lattice constants. In fact, subradiant modes can either be excited or inhibited

according to the periodicity. Hence, by tuning the periodicity of the array, one is able to control different optical responses even with the same type of building blocks. The experimental results agree well with the theoretical predictions.

The analysis of systems with an asymmetric spectral response presented in this work is very general and demonstrates that near-field coupling and symmetry-breaking are crucial factors for engineering planar plasmonic systems for specific applications. In particular, insights into the different coupling regimes at hand should be helpful for the design of efficient plasmonic surfaces for various applications, including plasmonic nanorulers, radiance based biosensors or optical metamaterials.

METHODS

In the experiments, an inverted dark field optical microscope equipped with an oil immersion $60\times$ objective with a numerical aperture of 1.45 (PLAPON 60xO TIRFM, Olympus) is used to record the reflectance spectra. The sample is placed on top of the objective on a piezoelectric stage. The illumination source is a halogen lamp and a polarizer is used to control the polarization of the beam. The angle of incidence is from the lateral side of the 1D array with TM polarization, so that there is no phase retardation across the 1D array; see Figure S4 (Supporting Information). The collection angle covers the half hemisphere on the reflection side to ensure complete angular-dependent output since the emission is anisotropic along y at the Fano resonance. The scattered light is collected by a spectrometer (Shamrock SR-303i, Andor) equipped with an electronic cooled CCD camera (iDus 401BRDD, Andor). The measured array length is around 2 μm, which is smaller than the coherent length of the light from the halogen lamp ($L_c = \lambda^2/\Delta\lambda = 720^2/240 \text{ nm} = 2.1 \ \mu$m).

Supporting Information Available: Additional figures explaining the coupling between two dolmen structures with different alignments and orientations together with far-field spectra; schematic illustration of the experimental setup for dark-field measurement. This material is available free of charge *via* the Internet at http://pubs.acs.org.

REFERENCES AND NOTES

1. Maier, S. A. *Plasmonics: Fundamentals and Applications*; Springer: New York, 2007
2. Sonnefraud, Y.; Verellen, N.; Sobhani, H.; Vandenbosch, G. A. E.; Moshchalkov, V. V.; Van Dorpe, P.; Nordlander, P.; Maier, S. A. Experimental Realization of Subradiant, Superradiant, and Fano Resonances in Ring/Disk Plasmonic Nanocavities. *ACS Nano* **2010**, *4*, 1664–1670.
3. Zhang, S.; Genov, D. A.; Wang, Y.; Liu, M.; Zhang, X. Plasmon-Induced Transparency in Metamaterials. *Phys. Rev. Lett.* **2008**, *101*, 047401.
4. Verellen, N.; Sonnefraud, Y.; Sobhani, H.; Hao, F.; Moshchalkov, V. V.; Dorpe, P. V.; Nordlander, P.; Maier, S. A. Fano Resonances in Individual Coherent Plasmonic Nanocavities. *Nano Lett.* **2009**, *9*, 1663–1667.
5. Hao, F.; Nordlander, P.; Sonnefraud, Y.; Dorpe, P. V.; Maier, S. A. Tunability of Subradiant Dipolar and Fano-Type Plasmon Resonances in Metallic Ring/Disk Cavities: Implications for Nanoscale Optical Sensing. *ACS Nano* **2009**, *3*, 643–652.
6. Mirin, N. A.; Bao, K.; Nordlander, P. Fano Resonances in Plasmonic Nanoparticle Aggregates. *J. Phys. Chem. A* **2009**, *113*, 4028–4034.
7. Miroshnichenko, A. E.; Flach, S.; Kivshar, Y. S. Fano Resonances in Nanoscale Structures. *Rev. Mod. Phys.* **2010**, *82*, 2257–2298.
8. Luk'yanchuk, B.; Zheludev, N. I.; Maier, S. A.; Halas, N. J.; Nordlander, P.; Giessen, H.; Chong, C. T. The Fano Resonance in Plasmonic Nanostructures and Metamaterials. *Nat. Mater.* **2010**, *9*, 707–715.
9. Gallinet, B.; Martin, O. J. F. Ab initio Theory of Fano Resonances in Plasmonic Nanostructures and Metamaterials. *Phys. Rev. B* **2011**, *83*, 235427.
10. Francescato, Y.; Giannini, V.; Maier, S. A. Plasmonic Systems Unveiled by Fano Resonances. *ACS Nano* **2012**, *6*, 1830–1838.
11. Liu, N.; Hentschel, M.; Weiss, T.; Alivisatos, A. P.; Giessen, H. Three-Dimensional Plasmon Rulers. *Science* **2011**, *332*, 1407–1410.
12. Gallinet, B.; Siegfried, T.; Sigg, H.; Nordlander, P.; Martin, O. J. F. Plasmonic Radiance: Probing Structure at the Ångström Scale with Visible Light. *Nano Lett.* **2012**, *13*, 497–503.
13. Zhang, Y.; Zhen, Y.-R.; Neumann, O.; Day, J. K.; Nordlander, P.; Halas, N. J. Coherent Anti-Stokes Raman Scattering with Single-Molecule Sensitivity Using a Plasmonic Fano Resonance. *Nat. Commun.* **2014**, *5*, 4424.
14. Le, F.; Brandl, D. W.; Urzhumov, Y. A.; Wang, H.; Kundu, J.; Halas, N. J.; Aizpurua, J.; Nordlander, P. Metallic Nanoparticle Arrays: A Common Substrate for Both Surface-Enhanced Raman Scattering and Surface-Enhanced Infrared Absorption. *ACS Nano* **2008**, *2*, 707–718.
15. Gallinet, B.; Martin, O. J. F. Refractive Index Sensing with Subradiant Modes: A Framework To Reduce Losses in Plasmonic Nanostructures. *ACS Nano* **2013**, *7*, 6978–6987.
16. Wu, C.; Khanikaev, A. B.; Adato, R.; Arju, N.; Yanik, A. A.; Altug, H.; Shvets, G. Fano-Resonant Asymmetric Metamaterials for Ultrasensitive Spectroscopy and Identification of Molecular Monolayers. *Nat. Mater.* **2012**, *11*, 69–75.
17. Gallinet, B.; Martin, O. J. F. Influence of Electromagnetic Interactions on the Line Shape of Plasmonic Fano Resonances. *ACS Nano* **2011**, *5*, 8999–9008.
18. Lovera, A.; Gallinet, B.; Nordlander, P.; Martin, O. J. F. Mechanisms of Fano Resonances in Coupled Plasmonic Systems. *ACS Nano* **2013**, *7*, 4527–4536.
19. Christ, A.; Ekinci, Y.; Solak, H. H.; Gippius, N. A.; Tikhodeev, S. G.; Martin, O. J. F. Controlling the Fano Interference in a Plasmonic Lattice. *Phys. Rev. B* **2007**, *76*, 201405.

20. Chen, J.; Shen, Q.; Chen, Z.; Wang, Q.; Tang, C.; Wang, Z. Multiple FanoResonances in Monolayer Hexagonal Non-Close-Packed Metallic Shells. *J. Chem. Phys.* **2012**, *136*, 214703–7.

21. Rodriguez, S. R. K.; Abass, A.; Maes, B.; Janssen, O. T. A.; Vecchi, G.; Gómez Rivas, J. Coupling Bright and Dark Plasmonic Lattice Resonances. *Phys. Rev. X* **2011**, *1*, 021019.

22. Wood, R. W. On a Remarkable Case of Uneven Distribution of Light in a Diffraction Grating Spectrum. *Proc. Phys. Soc. London* **1902**, *18*, 269.

23. Fano, U. The Theory of Anomalous Diffraction Gratings and of Quasi-Stationary Waves on Metallic Surfaces. *J. Opt. Soc. Am.* **1941**, *31*, 213–222.

24. Auguié, B.; Barnes, W. L. Collective Resonances in Gold Nanoparticle Arrays. *Phys. Rev. Lett.* **2008**, *101*, 143902.

25. Hicks, E. M.; Zou, S.; Schatz, G. C.; Spears, K. G.; Van Duyne, R. P.; Gunnarsson, L.; Rindzevicius, T.; Kasemo, B.; Käll, M. Controlling Plasmon Line Shapes through Diffractive Coupling in Linear Arrays of Cylindrical Nanoparticles Fabricated by Electron Beam Lithography. *Nano Lett.* **2005**, *5*, 1065–1070.

26. Kravets, V. G.; Schedin, F.; Grigorenko, A. N. Extremely Narrow Plasmon Resonances Based on Diffraction Coupling of Localized Plasmons in Arrays of Metallic Nanoparticles. *Phys. Rev. Lett.* **2008**, *101*, 087403.

27. Jiang, Y.-W.; Tzuang, L. D.; Ye, Y.-H.; Wu, Y.-T.; Tsai, M.-W.; Chen, C.-Y.; Lee, S.-C. Effect of Wood's Anomalies on the Profile of Extraordinary Transmission Spectra Through Metal Periodic Arrays of Rectangular Subwavelength Holes with Different Aspect Ratio. *Opt. Express* **2009**, *17*, 2631–2637.

28. Rodriguez, S. R. K.; Janssen, O. T. A.; Lozano, G.; Omari, A.; Hens, Z.; Rivas, J. G. Near-Field Resonance at Far-Field-Induced Transparency in Diffractive Arrays of Plasmonic Nanorods. *Opt. Lett.* **2013**, *38*, 1238–1240.

29. Shen, Y.; Zhou, J.; Liu, T.; Tao, Y.; Jiang, R.; Liu, M.; Xiao, G.; Zhu, J.; Zhou, Z.-K.; Wang, X.; *et al.* Plasmonic Gold Mushroom Arrays with Refractive Index Sensing Figures of Merit Approaching the Theoretical Limit. *Nat. Commun.* **2013**, *4*, 2381.

30. Ekinci, Y.; Christ, A.; Agio, M.; Martin, O. J. F.; Solak, H. H.; Löffler, J. F. Electric and Magnetic Resonances in Arrays of Coupled Gold Nanoparticle in-Tandem Pairs. *Opt. Express* **2008**, *16*, 13287–13295.

31. Liu, N.; Weiss, T.; Mesch, M.; Langguth, L.; Eigenthaler, U.; Hirscher, M.; Sönnichsen, C.; Giessen, H. Planar Metamaterial Analogue of Electromagnetically Induced Transparency for Plasmonic Sensing. *Nano Lett.* **2009**, *10*, 1103–1107.

32. Parsons, J.; Hendry, E.; Burrows, C. P.; Auguié, B.; Sambles, J. R.; Barnes, W. L. Localized Surface-Plasmon Resonances in Periodic Nondiffracting Metallic Nanoparticle and Nanohole Arrays. *Phys. Rev. B* **2009**, *79*, 073412.

33. Christ, A.; Martin, O. J. F.; Ekinci, Y.; Gippius, N. A.; Tikhodeev, S. G. Symmetry Breaking in a Plasmonic Metamaterial at Optical Wavelength. *Nano Lett.* **2008**, *8*, 2171–2175.

34. Zhang, W.; Fischer, H.; Schmid, T.; Zenobi, R.; Martin, O. J. F. Mode-Selective Surface-Enhanced Raman Spectroscopy Using Nanofabricated Plasmonic Dipole Antennas. *J. Phys. Chem. C* **2009**, *113*, 14672–14675.

35. Zhang, W.; Gallinet, B.; Martin, O. J. F. Symmetry and Selection Rules for Localized Surface Plasmon Resonances in Nanostructures. *Phys. Rev. B* **2010**, *81*, 233407.

36. Fedotov, V. A.; Rose, M.; Prosvirnin, S. L.; Papasimakis, N.; Zheludev, N. I. Sharp Trapped-Mode Resonances in Planar Metamaterials with a Broken Structural Symmetry. *Phys. Rev. Lett.* **2007**, *99*, 147401.

37. Hao, F.; Sonnefraud, Y.; Dorpe, P. V.; Maier, S. A.; Halas, N. J.; Nordlander, P. Symmetry Breaking in Plasmonic Nanocavities: Subradiant LSPR Sensing and a Tunable Fano Resonance. *Nano Lett.* **2008**, *8*, 3983–3988.

38. Hu, Y.; Noelck, S. J.; Drezek, R. A. Symmetry Breaking in Gold−Silica−Gold Multilayer Nanoshells. *ACS Nano* **2010**, *4*, 1521–1528.

39. Gallinet, B.; Martin, O. J. F. Relation Between Near-Field and Far-Field Properties of Plasmonic Fano Resonances. *Opt. Express* **2011**, *19*, 22167–22175.

40. Prodan, E.; Radloff, C.; Halas, N. J.; Nordlander, P. A Hybridization Model for the Plasmon Response of Complex Nanostructures. *Science* **2003**, *302*, 419–422.

41. Kern, A. M.; Martin, O. J. F. Surface Integral Formulation for 3D Simulations of Plasmonic and High Permittivity Nanostructures. *J. Opt. Soc. Am. A* **2009**, *26*, 732–740.

42. Gallinet, B.; Martin, O. J. F. Scattering on Plasmonic Nanostructures Arrays Modeled with a Surface Integral Formulation. *Phot. Nano. Fundam. Appl.* **2010**, *8*, 278–284.

43. Johnson, P. B.; Christy, R. W. Optical Constants of the Noble Metals. *Phys. Rev. B* **1972**, *6*, 4370–4379.

44. Kittel, C. *Introduction to Solid State Physics*; Springer-Verlag: New York, 1993.

45. Kottmann, J. P.; Martin, O. J. F.; David, R. S.; Sheldon, S. Field Polarization and Polarization Charge Distributions in Plasmon Resonant Nanoparticles. *New J. Phys.* **2000**, *2*, 27.

46. Kreibig, U. Electronic Properties of Small Silver Particles: the Optical Constants and Their Temperature Dependence. *J. Phys. F* **1974**, *4*, 999.